Toward Rational Design of Ribonuclease Inhibitors: High-Resolution Crystal Structure of a Ribonuclease A Complex with a Potent 3′,5′-Pyrophosphate-Linked Dinucleotide Inhibitor[†,‡]

Demetres D. Leonidas,[§] Robert Shapiro,[||,⊥] Laurence I. Irons,[§] Nello Russo,[||,#] and K. Ravi Acharya*[,§]

Department of Biology and Biochemistry, University of Bath, Claverton Down, Bath BA2 7AY, U.K., and Center for Biochemical and Biophysical Sciences and Medicine and Department of Pathology, Harvard Medical School, Boston, Massachusetts 02115

Received April 19, 1999; Revised Manuscript Received May 27, 1999

ABSTRACT: The crystal structure of ribonuclease A (RNase A) in complex with pdUppA-3′-p [5′-phospho-2′-deoxyuridine-3′-pyrophosphate (P′→5′) adenosine 3′-phosphate] has been determined at 1.7 Å resolution. This dinucleotide is the most potent low molecular weight inhibitor of RNase A reported to date (K_i = 27 nM) and is also effective against two major nonpancreatic RNases: eosinophil-derived neurotoxin and RNase-4; in all cases, tight binding in large part derives from the unusual 3′,5′-pyrophosphate internucleotide linkage [Russo, N., and Shapiro, R. (1999) *J. Biol. Chem. 274*, 14902−14908]. The design of pdUppA-3′-p was based on the crystal structure of RNase A complexed with 5′-diphosphoadenosine 3′-phosphate (ppA-3′-p) [Leonidas, D. D., Shapiro, R., Irons, L. I., Russo, N., and Acharya, K. R. (1997) *Biochemistry* 36, 5578−5588]. The adenosine of pdUppA-3′-p adopts an atypical syn conformation not observed for standard adenosine nucleotides bound to RNase A. This conformation, which allows extensive interactions with Asn 67, Gln 69, Asn 71, and His 119, is associated with the placement of the 5′-β-phosphate of the adenylate, rather than α-phosphate, at the site where substrate phosphodiester bond cleavage occurs. The contacts of the deoxyuridine 5′-phosphate portion of pdUppA-3′-p appear to be responsible for the 9-fold increased affinity of this compound as compared to ppA-3′-p: the uracil base binds to Thr 45 in the same manner as previous pyrimidine inhibitors, and the terminal 5′-phosphate is positioned to form medium-range Coulombic interactions with Lys 66. The full potential benefit of these added interactions is not realized because of compensatory losses of hydrogen bonds of Lys 7 and Gln 11 with the terminal 3′-phosphate and the adenylate 5′-α-phosphate, which were not predicted by modeling. The results reported here have important implications for the design of improved inhibitors of RNase A and for the development of therapeutic agents to control the activities of RNase homologues such as eosinophil-derived neurotoxin and angiogenin that have roles in human pathologies.

Numerous homologues of bovine pancreatic ribonuclease A (RNase A;[1] EC 3.1.27.5) have been shown to exhibit unusual biological activities in vivo. In some cases, these activities have pathological consequences: eosinophil-derived neurotoxin (EDN) and eosinophil cationic protein (ECP) are both neurotoxic, eliciting the Gordon phenomenon when injected into rabbits, and have been implicated in hypereosinophilic syndromes and allergy (*1*−*3*); human angiogenin (Ang) plays a critical role in the establishment of a wide range of human tumors through its capacity to induce neovascularization (*4*, *5*) and/or to serve as an adhesion molecule for tumor cells (*6*); and bovine seminal RNase (BS-RNase) has antispermatogenic and immunosuppressive activity (*7*−*9*). Other actions of these proteins are beneficial: EDN and ECP are helminthotoxic agents, and both of them possess antiviral activity (*10*−*12*). ECP also has bactericidal activity (*13*); Ang may be involved in normal angiogenesis, e.g., in wound healing; and both BS-RNase and the frog RNase onconase (ONC) inhibit tumor growth

[†] This work was supported by the Cancer Research Campaign [CRC] (U.K.) (Project Grant SP2354/0101 to K.R.A.), the Medical Research Council (U.K.) (Program Grant 9540039 to K.R.A.), the Wellcome Trust (U.K.) (Biomedical Research Collaboration Grant 044107/Z/95/Z to K.R.A. and R.S.), the Endowment for Research in Human Biology, Inc., Boston (R.S. and N.R.), and the Promega Corp., U.S.A. (R.S. and N.R.).

[‡] The atomic coordinates for the complex of ribonuclease A have been deposited with the Protein Data Bank (accession 1QHC).

* Address correspondence to this author at the Department of Biology and Biochemistry, University of Bath, Claverton Down, Bath BA2 7AY, U.K. Phone: +44-1225-826 238. Fax: +44-1225-826 779. E-mail: K.R.Acharya@bath.ac.uk.

[§] Department of Biology and Biochemistry, University of Bath.

[||] Center for Biochemical and Biophysical Sciences and Medicine, Harvard Medical School.

[⊥] Department of Pathology, Harvard Medical School.

[#] Present address: Dipartimento di Scienze della Vita, Seconda Università di Napoli, Via Arena 18, 81100 Caserta, Italy.

[1] Abbreviations: RNase A, bovine pancreatic ribonuclease A; Ang, angiogenin; EDN, eosinophil-derived neurotoxin; ECP, eosinophil cationic protein; BS-RNase, bovine seminal ribonuclease; pdUppA-3′-p, 5′-phospho-2′-deoxyuridine 3′-pyrophosphate (P′→5′) adenosine 3′-phosphate; ppA-3′-p, 5′-diphosphoadenosine 3′-phosphate; ppA-2′-p, 5′-diphosphoadenosine 2′-phosphate; 2′,5′-CpA, cytidylyl-2′,5′-adenosine; d(Up), 2′-deoxyuridine 3′-phosphate; UpA, uridylyl-(3′,5′)-adenosine; 2′,5′-UpA, uridylyl-(2′,5′)-adenosine; d(CpA), deoxycytidylyl-3′,5′-deoxyadenosine; UpcA, UpA with the 5′-oxygen of the adenosine ribose replaced by a methylene group; PEG, poly(ethylene glycol).

10.1021/bi990900w CCC: $18.00
Published on Web 07/22/1999

(*7, 14, 15*). Additional homologues may exhibit other physiological activities, as yet unknown. This seems particularly likely for human RNase-4, which was first isolated from colon carcinoma cells and blood plasma (*16*) and is detectable in white blood cells (*17, 18*). RNase-4 displays a high degree of amino acid sequence conservation (87−94%) across species (*19*) and has a unique specificity for uridine *(16*), suggesting that it may have an important biological role other than RNA degradation. In this regard, it may be significant that expression of RNase-4 mRNA has been found to correlate with differentiation of monocytes to macrophages (*18*) and human promyelocytic leukemia cells to neutrophils (*20*).

The vast majority of the unusual physiological activities of the RNase A homologues appear to be critically dependent on ribonucleolytic activity: i.e., these biological functions are lost when residues essential for ribonucleolysis are mutated or chemically modified or when assays are performed in the presence of RNase inhibitors. This has been shown for the angiogenic property of Ang (*21*−*23*), the neurotoxicity of EDN (*24, 25*), the antiviral action of EDN (*11*) and of ECP (*10*), the immunosuppressive activity of BS-RNase (*26*), and the antitumor activity of ONC (*27, 28*) and BS-RNase (*29*). These observations suggest that RNase inhibitors may prove valuable for identifying and studying the ribonucleolytically dependent biological actions of the various RNase homologues and may have utility as therapeutic agents in pathological conditions associated with some of these proteins.

All RNase homologues , like RNase A (*30, 31*), catalyze the cleavage of RNA by a transphosphorylation mechanism. However, their ribonucleolytic activities differ significantly both in magnitude and in specificity due to differences in the structures of their active sites. The central region of the catalytic site of RNase A consists of subsites P_1 (Gln 11, His 12, Lys 41, and His 119), B_1 (Thr 45, Asp 83, Phe 120, and Ser 123), and B_2 (Asn 67, Gln 69, Asn 71, Glu 111, and His 119). These subsites accommodate the phosphate where phosphodiester bond cleavage occurs (P_1) and the nucleotide bases on the 3′ and 5′ sides of the scissile bond (B_1 and B_2, respectively). In addition, chemical modification (*32*), kinetic (*33*), and site-directed mutagenesis experiments (*34*) have identified several peripheral sites, including P_0 (Lys 66) and P_2 (Lys 7 and Arg 10). P_0 interacts with the 5′-phosphate of a nucleotide bound at B_1, and P_2 interacts with the 3′-phosphate of a nucleotide bound at B_2 (for recent reviews, see refs *35*−*37*). The three catalytic residues His 12, Lys 41, and His 119 of the P_1 subsite are present in all RNase homologues. The key B_1 residue, Thr 45, is also maintained, but the other components of this subsite are variable. The B_2 subsite is fully or partially conserved in all of the other proteins. Subsites P_0 and P_2 are least conserved among RNase homologues. Despite cross-homologue differences in B_1 and B_2 site structures, all members of the RNase family bind only pyrimidines at B_1 and prefer purines at B_2. Thus, inhibitors designed to fit the $B_1-P_1-B_2$ core region of the active site of RNase A might be effective against the related RNases as well. In addition, ligands specific for each RNase could potentially be developed via structure-based strategies that exploit active site differences.

Efforts toward the rational design of low molecular weight inhibitors of RNases were initiated recently using RNase A as a model system. Two potent nucleotide inhibitors of RNase A, 5′-diphosphoadenosine 3′-phosphate (ppA-3′-p, K_i = 240 nM) and 5′-diphosphoadenosine 2′-phosphate (ppA-2′-p, K_i = 520 nM), were identified (*38*), and crystal structures for the complexes of RNase A with both compounds were determined (*39*). These inhibitors occupy the $P_1-B_2-P_2$ region of the active site in a manner that was not anticipated from earlier structures of RNase A complexes with d(ApTpApApG) (*40*), d(CpA) (*41, 42*), 2′,5′-CpA (*42*), and d(UpcA) (*43*). The key differences are (i) it is the 5′-β-phosphate rather than the 5′-α-phosphate of each 5′-diphospho inhibitor which occupies the P_1 site and (ii) the adenine ring of each 5′-diphospho inhibitor is rotated with respect to the other inhibitors, adopting a syn rather than an anti conformation. Based on these structural results, ppA-3′-p was extended by the addition of a 2′-deoxy-5′-phosphouridine to the β-phosphate group to produce pdUppA-3′-p [5′-phospho-2′-deoxyuridine 3′-pyrophosphate (P′→5′) adenosine 3′-phosphate] (*44*); the added substituents were targeted to the B_1 and P_0 subsites, which were not utilized by ppA-3′-p or ppA-2′-p. The new compound pdUppA-3′-p was found to be an even more potent inhibitor of RNase A than ppA-3′-p, with a K_i value of 27 nM, and is also effective against EDN and RNase-4 [K_i values are 180 nM and 260 nM, respectively (*44*)]. Here we present a high-resolution (1.7 Å) crystal structure of the RNase A−pdUppA-3′-p complex which reveals the molecular interactions at the active site and suggests ways to develop RNase A inhibitors that might bind more tightly still. In addition, modeling of the complexes of pdUppA-3′-p with EDN and RNase-4 indicates how this pyrophosphate-linked dinucleotide might bind and suggests strategies for tailoring such inhibitors to be specific for these RNases.

EXPERIMENTAL PROCEDURES

The preparation of pdUppA-3′-p was performed as described (*44*) except that the final sample was converted from the triethylammonium to the sodium salt by passing it through a column of SP-Sephadex (Na^+) resin in water. Diffraction data to 1.7 Å resolution were collected from a single monoclinic RNase A crystal at room temperature on a 30 cm MAR-Research image plate using synchrotron radiation at the SRS (Daresbury, U.K.). The crystal was grown as described previously (*39*), and soaked for 4.5 days in 20 mM pdUppA-3′-p, 20 mM sodium citrate, pH 5.5, 25% PEG 4000. Additional data sets (one at 1.9 Å and one at 3.0 Å resolution) were collected from a single RNase A crystal soaked with pdUppA-3′-p as described on a 30 cm MAR-Research image plate mounted on an Enraf-Nonius rotating-anode X-ray source with Cu Kα radiation. Auto-indexing and data processing were performed with DENZO and SCALEPACK (*45*). All data sets were merged together (R_m = 0.083) to give a final data set comprising 25 666 unique reflections, 94.5% complete to 1.7 Å resolution. Phases were obtained using the structure of free RNase A (*39*) as a starting model. Alternating cycles of manual building, conventional positional refinement, the simulated annealing method, and finally solvent correction as implemented in X-PLOR 3.851 (*46*) improved the model. The inhibitor molecule was included during the final stages of refinement using the

Table 1: Crystallographic Statistics

space group	*C*2 (two molecules per asymmetric unit)		
cell dimensions	$a = 101.4$ Å, $b = 33.2$ Å, $c = 73.1$ Å, $\beta = 90.11°$		
wavelength (Å)	1.5418	1.5418	1.488
resolution (Å)	40.0−3.0	35.0−1.9	30.0−1.7
no. of reflections measured	11893	64067	99040
no. of unique reflections	4544	19113	21506
completeness (%) (outermost shell)	87.6 (73.6)	95.9 (84.6)	79.0 (84.0)
R_{symm}[a] (%)	5.3	6.5	7.1
total no. of unique reflections		25723	
R_{merge}[b] (%)		8.3	
overall completeness (%)		94.5	
$I/\sigma I$		5.7	
no. of reflections used in refinement (20−1.7 Å) ($F > 0$)		25666	
R_{cryst}[c] (%)		20.0	
R_{free}[d] (%)		26.0	
no. of protein atoms		1902	
no. of solvent molecules		137	
no. of inhibitor atoms		100	
deviations from ideality (rms)			
bond lengths (Å)		0.01	
bond angles (deg)		1.4	
dihedrals (deg)		27.3	
impropers (deg)		0.8	
average *B* factor (Å^2)			
main-chain atoms (mol I/mol II)		29.6/28.7	
side-chain atoms (mol I/mol II)		31.9/30.8	
all protein atoms (mol I/mol II)		30.7/29.7	
solvent atoms		47.9	
inhibitor molecules (mol I/mol II)		42.9/51.5	

[a] $R_{symm} = \sum_h\sum_i|I(h) - I_i(h)|/\sum_h\sum_i I_i(h)$, where $I_i(h)$ and $I(h)$ are the *i*th and the mean measurements of the intensity of reflection *h*. [b] R_{merge} is equal to R_{symm}, but it refers to merging data from different crystals and different sources. [c] $R_{cryst} = \sum_h|F_o - F_c/\sum_h F_o$, where F_o and F_c are the observed and calculated structure factor amplitudes of reflection *h*, respectively. [d] R_{free} is equal to R_{cryst} for a randomly selected 5% subset of reflections not used in the refinement (*48*).

atomic coordinates of ppA-3′-p from the crystal structure of the RNase A−ppA-3′-p complex (PDB 1afk) (*39*) and the coordinates of uridine vanadate (UVan) from the crystal structure of the RNase A−UVan complex (PDB 1ruv) (*47*). The final model comprising 2 RNase A molecules, 2 pdUppA-3′-p molecules, and 137 water molecules was refined to $R_{cryst} = 0.20$ and $R_{free} = 0.26$ (*48*). Details of data processing and refinement statistics are presented in Table 1.

RESULTS AND DISCUSSION

Conformation of pdUppA-3′-p When Bound to RNase A. There are two RNase A molecules in the asymmetric unit in the crystal, and the inhibitor is bound to both of them. All atoms of pdUppA-3′-p are well-defined in the electron density map in both monomers of the noncrystallographic dimer (the inhibitor in RNase molecule I is shown in Figure 1). The conformation of the adenosine moiety is very similar to that observed in the ppA-3′-p complex (Figure 2) (*39*), with the glycosyl torsion angle χ' in the syn range (Figure 3, Table 2). Although free adenosine nucleotides show a small preference for syn conformations (*49*), this conformation is rare in protein-bound adenosines, and has been observed previously only in the RNase−ppA-2′-p/ppA-3′-p (*39*) and fructose-1,6-bisphosphatase−AMP (*50*) complexes. Torsion angle β in adenosine (Figure 3) is in the $-ac$ range. This is very different from that observed in ppA-3′-p ($+ac$) but similar to that in ppA-2′-p ($-ac$) (*39*). The γ torsion angle in adenosine is in the $+sc$ range as usually found in free nucleotides and differs considerably from those in the ppA-3′-p and ppA-2′-p complexes (both $-sc$). The C5′A-O5′A- PA plane is rotated by ~60° with respect to that in ppA-3′-p, moving atom PA approximately 1.6 Å away from its position in the RNase A−ppA-3′-p complex (Figure 2) and bringing the entire α-phosphate group closer to the adenine ring. [The nomenclature used here for the two phosphate components of the pyrophosphate of pdUppA-3′-p is the same as for ppA-3′-p (*39*): i.e., α and β are with

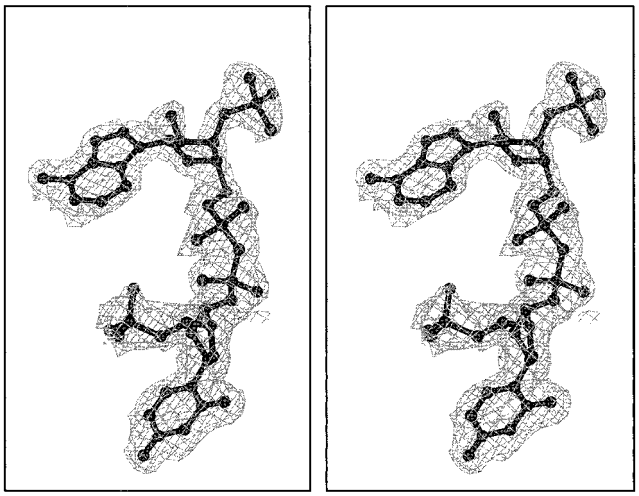

FIGURE 1: Stereo diagram of a 1.7 Å SigmaA $2|F_o| - |F_c|$ electron density map calculated using the standard protocol as implemented in X-PLOR 3.851 (*76*) from the RNase model before incorporating the coordinates of pdUppA-3′-p. The map is contoured at the 2.0 σ level. The refined structure of pdUppA-3′-p (from molecule I) is shown.

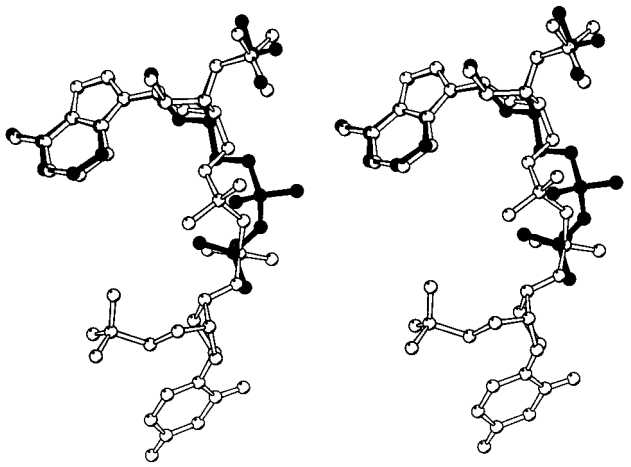

FIGURE 2: Stereoview of the superimposed structures of pdUppA-3′-p (white, from molecule I) and ppA-3′-p (black) (*39*) when bound to RNase A.

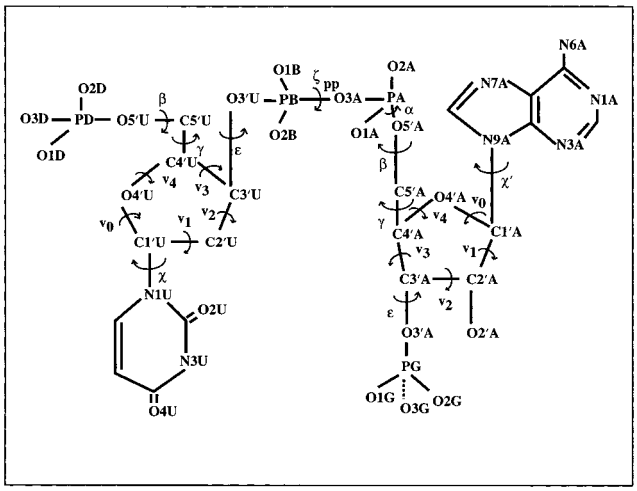

FIGURE 3: Numbering scheme and torsion angle assignment for pdUppA-3′-p (*49*).

respect to the adenosine (Figure 3).] Nevertheless, the β-phosphate occupies a position almost identical to that of the β-phosphate in the ppA-3′-p complex. The glycosyl torsion angle χ of the uridine is in the anti range (Figure 3, Table 2), as found in most free and protein-bound pyrimidine nucleotides (*49*). Torsion angles β and γ of the uridine (Figure 3) are in the $-ac$ and $+sc$ range, respectively, and are similar to the β and γ angles of the adenosine. Both adenosine and uridine ribose rings adopt the *C2′-endo* puckering, one of the two furanose puckerings most frequently observed in free and bound nucleotides (the other is *C3′-endo*) (*49*). The two monophosphate groups attached to the 3′- and 5′-positions of adenosine and uridine, respectively, point away from the backbone of the inhibitor in opposite directions. These phosphate groups, like the 3′-phosphate in ppA-3′-p, appear to be mobile and have high-temperature factors in both RNase A molecules (50−60 Å^2) in comparison to the rest of the inhibitor atoms.

Interactions of pdUppA-3′-p with RNase A. The inhibitor pdUppA-3′-p binds to the active site of RNase A by displacing six water molecules found in the free structure (*39*), with the adenosine-3′,5′-diphosphate portion occupying the B_2 and P_2 subsites and the uridine-3′,5′-diphosphate moiety binding to B_1, P_1, and P_0 (Figure 4A,B). The contacts of adenosine with the protein (Table 3) are nearly identical to those observed for the ppA-3′-p complex (*39*). N6A and N7A form hydrogen bonds with Asn 71 in both molecules of the noncrystallographic dimer. In molecule I, N6A makes an additional hydrogen bond with Gln 69, whereas in molecule II it interacts with Asn 67. To form the Gln 69/N6A hydrogen bond in molecule I, Gln 69 has tilted slightly from its conformation in the free RNase structure, thereby losing an interaction with the side chain of Asn 71. The six-membered ring of the adenine forms stacking interactions with the imidazole ring of His 119 (Figure 4B). There are also numerous van der Waals contacts between adenosine and Cys 65, Asn 67, Gln 69, Asn 71, Ala 109, Glu 111, and Val 118 (Table 4).

The β-phosphate group of pdUppA-3′-p binds to subsite P_1 in a manner similar to that in the RNase A−ppA-3′-p complex, and is involved in a hydrogen bond network with the side chains of Gln 11, His 12, and His 119 and the main chain of Phe 120 (Table 3, Figure 4B). In molecule I of the noncrystallographic dimer, the β-phosphate also hydrogen bonds to the side chain of Lys 41, as in the ppA-3′-p complex. The position of this phosphate is very close to that occupied by the oxyvanadate anion in the complex of RNase A with the transition state analogue UVan (*47*, *51*). The differences between the positions of PB and the vanadium atom in molecules I and II are 0.3 and 0.5 Å, respectively. In the ppA-3′-p complex, the α-phosphate hydrogen bonds with Gln 11 in both molecules, and with Lys 7 as well in molecule II (*39*); in addition, O5′ hydrogen bonds with Lys 7 in both molecules. The interactions with Gln 11 are not replicated in the pdUppA-3′-p complex because of the marked differences in the α and β torsion angles of adenosine (see above), although one of the two hydrogen bonds with Lys 7 in molecule II still forms. The α-phosphate also appears to hydrogen bond with a β-phosphate oxygen, as observed in the RNase−ppA-2′-p complex.

The uridine of pdUppA-3′-p binds in subsite B_1 with the uracil forming two hydrogen bonds with Thr 45 and packing against the phenyl ring of Phe 120 (Table 3, Figure 4B) in a manner almost identical to that in the RNase A−UVan complex (*47*) and in other RNase complexes with uridylyl nucleotides (*43*). Two water molecules mediate interactions between uracil and Asp 83 and Ser 123: one forms hydrogen bonds with atoms O4U of uracil, Oδ1 of Asp 83, and Oγ of Ser 123; the second interacts with O4U of uracil and the main-chain nitrogen of Ser 123 (Figure 4B). Both waters are well-defined in the electron density map and are involved in similar interactions in both molecules of the noncrystallographic dimer. These water molecules might correspond to those observed by Gilliland et al. (*52*) that were proposed to adjust their donor/acceptor hydrogen bonding roles depending on whether uracil or cytosine is bound at the B_1 subsite (atom Oγ of Thr 45 also changes its role to accommodate either pyrimidine). In the RNase A−pdUppA-3′-p complex, Oγ of Thr 45 also hydrogen bonds to the side chain of Asp 83; such an interaction was found previously in uridine (*53*) but not in cytidine complexes (*41*), and mutational results (*54*, *55*) indicate that it strengthens preferentially the binding of uracil. The uridine 2′-deoxy sugar adopts a *C2′-endo* puckering similar to that seen for cytidine in the RNase−d(CpA) complex (*41*), and for

Table 2: Torsion Angles for pdUppA-3′-p When Bound to RNase A[a]

	pdUppA-3′-p			
	adenosine		2′-deoxyuridine	
torsion angles[b] (deg)	molecule I	molecule II	molecule I	molecule II
backbone torsion angles				
O5′(A/U)-C5′(A/U)-C4′(A/U)-C3′(A/U) (γ)	52 (+*sc*)	48 (+*sc*)	65 (+*sc*)	59 (+*sc*)
C5′(A/U)-C4′(A/U)-C3′(A/U)-O3′(A/U) (δ)	140 (+*ac*)	140 (+*ac*)	148 (+*ac*)	142 (+*ac*)
C5′(A/U)-C4′(A/U)-C3′(A/U)-C2′(A/U)	−104	−108	−95	−98
C4′A-C3′A-C2′A-O2′A	−155	−153		
glycosyl torsion angle				
O4′U-C1′U-N1U-C2U (χ)			−130 (*anti*)	−133 (*anti*)
O4′A-C1′A-N9A-C4A (χ')	85 (*syn*)	88 (*syn*)		
pseudorotation angles				
C4′(A/U)-O4′(A/U)-C1′(A/U)-C2′(A/U) (υ_0)	−32	−34	−22	−16
O4′(A/U)-C1′(A/U)-C2′(A/U)-C3′(A/U) (υ_1)	41	43	36	30
C1′(A/U)-C2′(A/U)-C3′(A/U)-C4′(A/U) (υ_2)	−34	−35	−35	−31
C2′(A/U)-C3′(A/U)-C4′(A/U)-O4′(A/U) (υ_3)	17	16	24	22
C3′(A/U)-C4′(A/U)-O4′(A/U)-C1′(A/U) (υ_4)	9	11	−2	−4
phase	148	146	163	168
	C2′-endo	*C2′-endo*	*C2′-endo*	*C2′-endo*
phosphate torsion angles				
O3A-PA-O5′A-C5′A (α)	−58 (−*sc*)	−72 (−*sc*)		
P(A/D)-O5′(A/U)-C5′(A/U)-C4′(A/U) (β)	−136 (−*ac*)	−121 (−*ac*)	−142 (−*ac*)	−150 (−*ac*)
P(G/B)-O3′(A/U)-C3′(A/U)-C4′(A/U) (ϵ)	−103 (−*ac*)	−75 (−*sc*)	−82 (−*sc*)	−88 (−*sc*)
P(B/G)-O3′(A/U)-C3′(A/U)-C2′(A/U)	146	175	166	156
PB−O3A-PA-O5′A (ζ_{pp})	−95 (−*ac*)	−77 (−*sc*)		

[a] Definitions of the torsion angles are according to the current IUPAC−IUB nomenclature (*73*), and the phase angle of the ribose ring is calculated as described previously (*74*). [b]For atom definitions, see Figure 3.

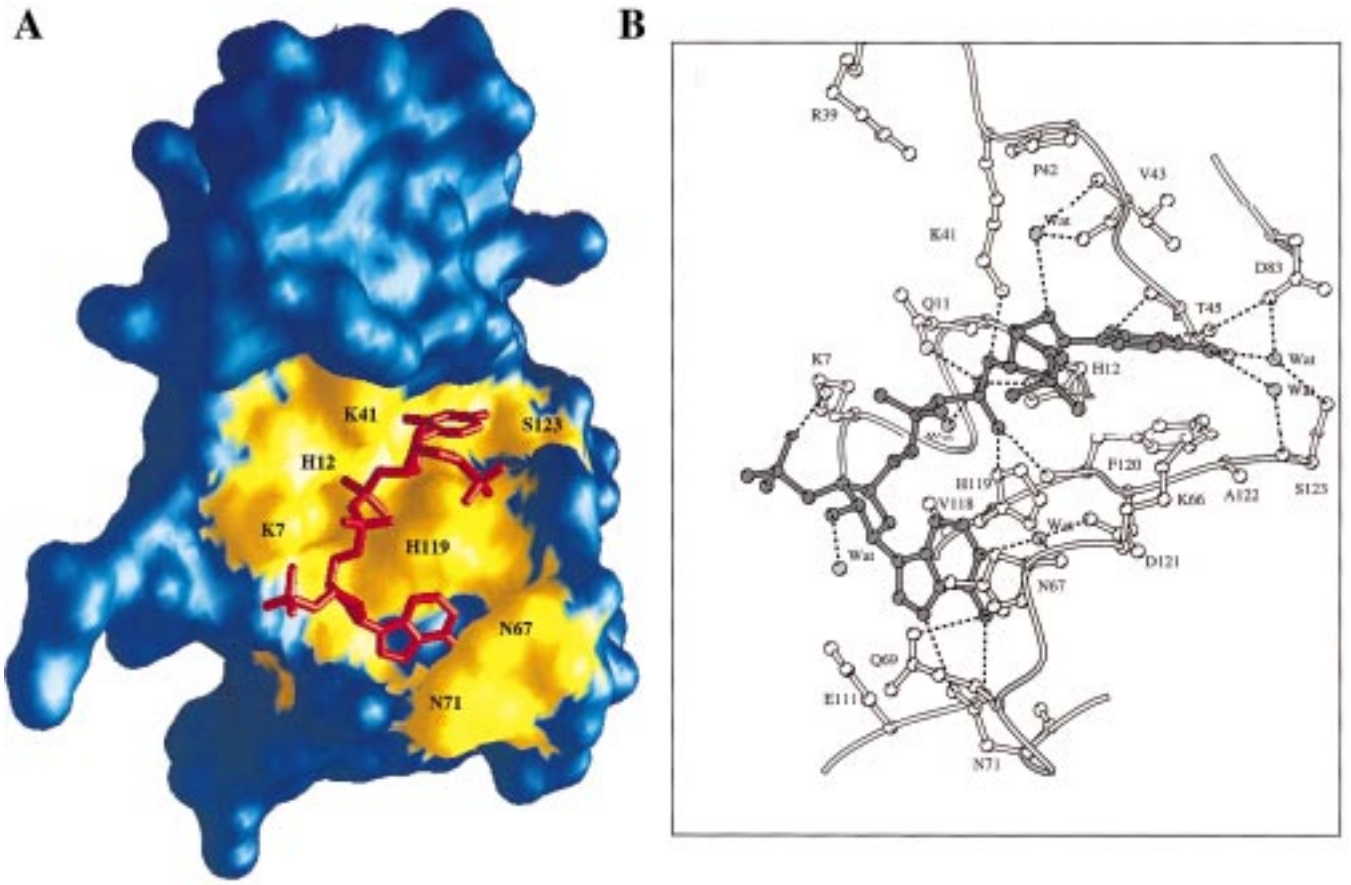

FIGURE 4: (A) Molecular surface of RNase A calculated using the program GRASP (*77*). The inhibitor pdUppA-3′-p is shown in red as a ball-and-stick model. The RNase residues interacting with pdUppA-3′-p are shown in yellow. (B) Interactions of pdUppA-3′-p with RNase A in molecule I. RNase residues are drawn as ball-and-stick models, water molecules as black spheres, and the inhibitor molecule is shown in black. Hydrogen bonds are indicated by dashed lines. Diagram drawn with MOLSCRIPT (*78*).

thymidine in the RNase−d(ApTpApApG) complex (*40*). This is in contrast to those of uridine in the UVan (*C3′-endo*) (*51*) and d(UpcA) (*C3′-exo*) (*43*) complexes and for cytidine in the RNase−2′,5′-CpA complex (*C4′-exo*) (*42*).

Table 3: Hydrogen Bond Interactions of pdUppA-3′-p in the Crystal[a]

donor	acceptor	RNase molecule I	RNase molecule II
Lys 7 Nζ	O3G	2.7	–
Lys 7 Nζ	O1A	–	2.8
Gln 11 Nϵ2	O2B	2.9	2.6
His 12 Nϵ2	O2B	2.4	2.6
Lys 41 Nζ	O3′U	3.1	–
Thr 45 N	O2U	2.8	3.0
N3U	Thr 45 Oγ1	2.8	2.7
N6A	Asn 67 Oδ1	–	3.3
N6A	Gln 69 Oϵ1	3.2	–
N6A	Asn 71 Oδ1	3.1	3.2
Asn 71 Nδ2	N7A	3.2	3.3
His 119 Nδ1	O1B	2.8	2.6
Phe 120 N	O1B	2.9	3.2
water	O2B	2.7	2.9
N1A	water	2.9	2.6
water	O2′A	3.5	2.6
water	O4′U	3.4	3.4
water	O4U	3.4	2.8
water	O4U	2.8	3.1
Thr 70 Oγ1[b]	O2′A	3.1	–
O2G	Gly 88 O[b]	3.1	–
water[b]	O3′A	–	3.3
water[b]	O3G	–	2.8

[a] Hydrogen bond interactions were calculated with the program HBPLUS (*75*). Values shown are distances in angstroms. [b] Atoms from a symmetry molecule.

Several early kinetic studies (*33, 56*−*58*) showed that a P_0 phosphate binding subsite exists in RNase A, and, based on modeling (*59*) and evolutionary considerations (*60, 61*), it was later proposed that Nζ of Lys 66 constitutes this site. In the only previous crystallographic study of RNase A in complex with a nucleotide expected to occupy the P_0 site [d(ApTpApApG)], Lys 66 did not form any hydrogen bonds with the P_0 phosphate and was found to be involved in crystal packing contacts instead (*40*). However, it was suggested that in solution Lys 66 might adopt a conformation which would allow this hydrogen bond to form. Most recently, Fisher et al. (*62*) demonstrated that the RNase A variant K66A displays 3-fold reduced catalytic efficiency toward poly(C) and severalfold weaker nucleic acid binding, consistent with a role for Lys 66 as a component of P_0. They proposed that the interactions between the amino group and the phosphate are only Coulombic. In the RNase A−pdUppA-3′-p complex determined here, the position of the Nζ atom of Lys 66 is well-defined in the electron density map in molecule I, but in molecule II there is no density for this residue beyond the Cβ atom. The distance between Nζ of Lys 66 (in molecule I) and the nearest oxygen of the 5′-phosphate is ∼4.7 Å, again too long for a hydrogen bond but well within the range where significant Coulombic forces may exist. It should be noted that Lys 66 is not involved in any crystal packing contacts in this structure and that its conformation is similar to that in free RNase A and in the ppA-3′-p (*39*), UpcA (*43*), and d(CpA) (*41*) complexes. In all of these cases, the side chain of Lys 66 forms a hydrogen bond with the main-chain oxygen of Asp 121.

In subsite P_2 of molecule I, Nζ of Lys 7 has moved from its position in free RNase A (*39*) to one which allows it to form a hydrogen bond with O1G (Table 3). However, in molecule II this atom is oriented so as to interact with O1A rather than O1G, and there are no direct hydrogen bonds involving the 3′-phosphate (Table 3). In the ppA-3′-p complex, Lys 7 hydrogen bonds to O1G in both molecules and to O1A as well in molecule II. This difference between molecules I and II correlates with differences in the conformations of the 3′-phosphate in the two molecules, which reflect the mobility of the phosphate group as described above. The side chain of Lys 7 appears to have a high degree of flexibility in general since it adopts distinct conformations in each RNase molecule of the noncrystallographic dimer in the ppA-2′-p, ppA-3′-p, and pdUppA-3′-p complexes as well as in free RNase A. The other residue implicated in the P_2 subsite, Arg 10, is ∼8 Å away from the 3′-phosphate of the inhibitor, and may form weak Coulombic interactions with it, as it is proposed to do with polynucleotide RNA substrates (*62*).

In all, pdUppA-3′-p is involved in 11 and 10 hydrogen bonds with RNase A in molecules I and II, respectively, and 6 with water in each molecule (Table 3, Figure 4B); 4 of these water molecules mediate interactions between RNase and pdUppA-3′-p (3 to uridine and 1 to adenine). The inhibitor ppA-3′-p forms a similar number of hydrogen bonds with the enzyme (11 in both molecule I and molecule II) but fewer with water [5 (molecule I) and 3 (molecule II)] (*39*). Five (molecule I) and three (molecule II) well-defined water molecules in the active site of the ppA-3′-p complex are displaced by the additional uridine moiety of the new inhibitor. pdUppA-3′-p forms 59 and 51 van der Waals interactions with 14 and 13 RNase residues in molecules I and II, respectively (Table 4, Figure 4A). In comparison, ppA-3′-p makes 41 (molecule I) and 58 (molecule II) van der Waals contacts with 10 and 11 residues, respectively (*39*).

Modeling of pdUppA-3′-p Binding to EDN and RNase-4. pdUppA-3′-p is an effective inhibitor of EDN and RNase-4 with K_i values of 180 nM and 260 nM, respectively (*44*). To examine how the inhibitor might bind to these other RNases, we have superimposed the present complexed structure onto the crystal structures of EDN (*63*) and the RNase-4−d(Up) complex [PDB 3rnf (*64*)].

The structure of EDN in complex with sulfate has been determined at 1.83 Å resolution (*63*). Two protein-bound sulfate anions were identified: one binds in subsite P_1, while the other occupies a site which was suggested to correspond to a P_{-1} phosphate binding subsite (*63*). P_1 is entirely conserved between EDN and RNase A, with EDN residues Gln 14, His 15, Lys 38, and His 129 corresponding to RNase residues Gln 11, His 12, Lys 40, and His 119, respectively. In subsites B_1 and B_2, residues Thr 45, Asn 67, and Asn 71 of RNase A are maintained in EDN as Thr 42, Asn 65, and Asn 70, whereas Gln 69, Asp 83, Glu 111, Phe 120, and Ser 123 are replaced by Arg 68, His 82, Asp 112, Leu 130, and Ile 133, respectively. Examination of the EDN−pdUppA-3′-p model suggests that seven water molecules in the active site would be displaced by the inhibitor. With the exception of the 3′-phosphate (see below), the inhibitor can be accommodated in the P_0−B_1−P_1−B_2−P_2 region of the active site without any conflict (Figure 5A). Most of the interactions at B_1 and P_1 are nearly identical to those in the pdUppA-3′-p−RNase A complex. The uridine and pyrophosphate moieties of pdUppA-3′-p are within hydrogen bonding distance of Thr 42 of the B_1 subsite and Gln 14, His 15, and Leu 130 (N) of the P_1 subsite, respectively. Also, the β-phosphate is very close to the position of the P_1 sulfate

Table 4: van der Waals Interactions between pdUppA-3′-p and RNase A in the Crystal[a]

	RNase A residues (no. of contacts)	
inhibitor atom	molecule I	molecule II
PB	His 12 (1)	–
O1B	His 119 (3)	His 119 (2)
O2B	His 12 (2)	His 12 (1)
O3G	Lys 7 (1)	Lys 7 (1)
C4A	His 119 (2)	His 119 (2)
N3A	His 119 (3)	His 119 (2)
C2A	His 119 (5)	Asn 67 (1), His 119 (5)
N1A	Asn 67 (2), His 119 (1)	Asn 67 (2), His 119 (1)
C6A	Asn 67 (2), Gln 69 (1), Ala 109 (1), His 119 (1)	Asn 67 (2), Gln 69 (1), Ala 109 (1)
N6A	Cys 65 (2), Asn 67 (1), Gln 69 (1)	Cys 65 (2), Asn 67 (1), Gln 69 (2), Ala 109 (2)
C5A	Gln 69 (1), Ala 109 (1)	Ala 109 (1)
N7A	Ala 109 (1)	Asn 71 (1), Ala 109 (1)
C8A	Glu 111 (2), V118 (1)	Val 118 (1)
C5′A	Val 118 (3), His 119 (1)	Lys 7 (1), Val 118 (2), His 119 (1)
C4′A	Val 118 (1)	Val 118 (1)
O4′A	Val 118 (1), His 119 (1)	His 119 (1)
C4′U	Lys 41 (2)	–
C1′U	Lys 41 (1)	–
C2′U	Phe 120 (1)	Phe 120 (1)
C3′U	–	His 119 (1)
C2U	Asn 44 (1), Thr 45 (1), Phe 120 (1)	Asn 44 (1), Thr 45 (1), Phe 120 (1)
O2U	His 12 (1), Asn 44 (2)	His 12 (1), Asn 44 (1)
N3U	Thr 45 (1), Phe 120 (1)	Thr 45 (1), Phe 120 (2)
C4U	Val 43 (1), Thr 45 (1), Phe 120 (2)	Thr 45 (1), Phe 120 (2)
C5U	Val 43 (1)	–
total	59 (14 RNase residues)	51 (13 RNase residues)

[a] van der Waals distances are calculated using van der Waal contact radii for atoms: C, 2.05 Å; O, 1.54 Å; N, 1.7 Å; S, 1.85 Å; and P, 1.9 Å.

anion found in the EDN crystal structure. In the B_2 site, atoms N6A and N7A of adenine are ~3.5 Å from the side-chain amide of Asn 70, and minor positional shifts would allow hydrogen bonds to form as for Asn 71 in the RNase A complex. However, the side chains of Asn 65 and Arg 68 are linked by a hydrogen bond, and in contrast to their RNase A structural counterparts, Asn 67 and Gln 69, point away from the adenine.

In free RNase A, His 119 adopts two distinct conformations, A and B (*65, 66*). Conformation B is incompatible with occupation of the B_2 site, and in complexes of RNase A with dinucleotides and polynucleotides, His 119 is always found in conformation A. In the free EDN crystal structure, His 129 is in conformation B (*63*), but in order for binding of pdUppA-3′-p to occur, it would have to shift to conformation A to avoid clashes with the inhibitor. In this case, it would form hydrogen bonds with the β-phosphate of the inhibitor and stacking interactions with adenine as in the RNase A complex.

In the modeled EDN complex, one of the 5′-phosphate oxygens of pdUppA-3′-p is 4.4 Å away from atom Oγ of Ser 64. However, small reorientations of the serine side chain and the phosphate could move these atoms within hydrogen bonding distance. Changes in the conformations of the side chains of Asp 131 and Arg 132, which are 6.7 and 5.6 Å, respectively, from the nearest 5′-phosphate oxygens in the model, could allow them to hydrogen bond to the phosphate as well. The participation of Arg 132 in the P_0 subsite of EDN was proposed previously by Beintema (*61*). Even without any reorientation, Arg 132 could contribute to binding of the 5′-phosphate through Coulombic interactions as for Lys 66 of RNase A.

The most surprising element in the pdUppA-3′-p−EDN model is that the 3′-phosphate passes directly through the aromatic ring of Trp 7 (Figure 5A). Attempts to resolve this conflict by altering either the puckering of the ribose or the conformation of the phosphate were unsuccessful. Energy minimization of the model, with the coordinates of pdUppA-3′-p kept fixed, resulted in shifts of the main-chain and side-chain atoms of Trp 7 by 0.7−1.1 and 3.0−5.5 Å, respectively, from their positions in the free EDN structure (Figure 5B). This conformational change, which did not affect the secondary structure of EDN (Trp 7 is still part of an α-helix), resolved the steric clash and placed the Trp 7 side chain in a position where it could engage in van der Waals contacts with the adenosine ribose of the inhibitor. Given the high affinity of pdUppA-3′-p for EDN (*44*), it seems likely that Trp 7 adopts this (or another nonobstructive) orientation rather than that in the crystal structure of free EDN when the inhibitor binds. Moreover, it should be noted that in natural EDN, which was used for the kinetic studies on pdUppA-3′-p binding (*44*), Trp 7 is mannosylated at CD1 (*67*), whereas the recombinant protein crystallized by Mosimann et al (*63*) was not. The conformation of the C-mannosylated residue in free, authentic EDN may differ from that seen in the crystal structure, and it may not be necessary for Trp 7 to be repositioned when pdUppA-3′-p binds.

The present model suggests several modifications of pdUppA-3′-p that might enhance its affinity for EDN. Suitable groups attached to the uridine ribose might be able to interact with Arg 36, Asn 39, and Gln 40 in the putative P_{-1} subsite of EDN in the same manner as one of the sulfate ions in the crystal structure (*63*). Indeed, such inhibitor substituents might favor binding to EDN since Asn 39 and Gln 40 are nonconservatively replaced in pancreatic RNase and most other homologues . In addition, it may be possible to extend pdUppA-3′-p from the terminal 5′-phosphate or

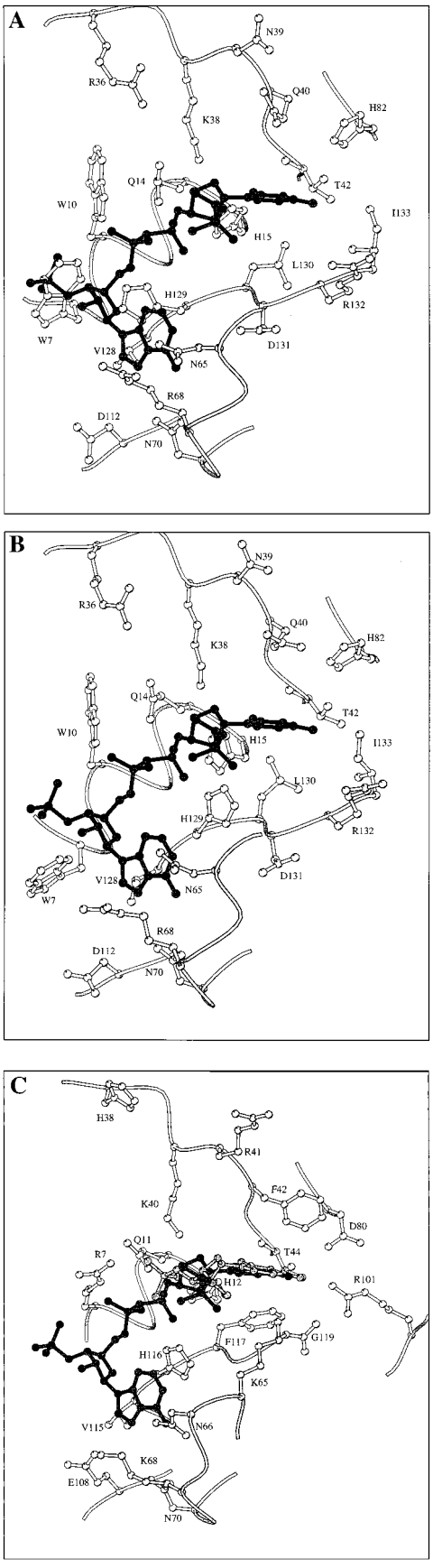

FIGURE 5: Modeled complexes of pdUppA-3′-p with EDN [before (A) and after energy minimization (B)] and with RNase-4 (C). Protein residues are in white, and pdUppA-3′-p is in black. The view is similar to that in Figure 4B. Also shown in gray, d(Up) in the active site of RNase-4 (C). Diagrams drawn with MOLSCRIPT (*78*).

the adenosine 2′-hydroxyl so as to form strong interactions with Arg 132 or Asp 112, respectively.

The crystal structures of RNase-4 and its complex with d(Up) were determined recently at 2.1 and 2.4 Å resolution, respectively (*64*). The majority of the subsites of RNase A are maintained in RNase-4: there are no sequence differences involving P_1 and P_0, with a single conservative replacement at P_2 (Arg 7 for Lys 7) and one substitution in B_2 (Lys 68 for Gln 69). However, the B_1 site of RNase-4 differs from that of RNase A more significantly, reflecting the unique and highly stringent specificity of this enzyme for uridine nucleotides (*16*): Val 43, which forms one face of this site in RNase A, is replaced by Phe 42; Ser 123 of RNase A is deleted [the other B_1 components in RNase A (Thr 45, Asp 83, and Phe 120) are conserved as Thr 44, Asp 80, and Phe 117]. Moreover, the crystal structure of the RNase-4 complex with d(Up) shows that Arg 101 of RNase-4 penetrates into the B_1 recognition pocket, whereas its counterpart in RNase A does not; Arg 101 interacts directly with atom O4 of uracil and forms multiple contacts with other residues that favor binding of this pyrimidine over cytosine. Consistent with these observations, mutation of Arg 101 has been demonstrated to reduce activity toward UpA by 385-fold while barely affecting cleavage of CpA (*68*).

Superposition of the present RNase A−pdUppA-3′-p complex structure onto that of the RNase-4−d(Up) complex gives an rms deviation of 1.2 Å in the C^{α} positions for 117 equivalent residues. Inspection of the superimposed structures suggests that pdUppA-3′-p can be accommodated in the RNase-4 active site without any steric conflicts (Figure 5C). However, the two inhibitor molecules are oriented somewhat differently. O4U and N3U of pdUppA-3′-p are 0.9 and 0.6 Å, respectively, from their equivalents in d(Up); as a result, these pdUppA-3′-p atoms are 3.7 and 3.0 Å away from Arg 101 and Thr 44, respectively, whereas O4 and N3 of d(Up) are only 2.9 and 2.6 Å from these residues. The β-phosphate of pdUppA-3′-p is ~2.0 Å from the 3′-phosphate of d(Up), but could potentially form the same type of interactions with the P_1 site (hydrogen bonds with Gln 11, His 12, His 116, and Phe 117) as in the RNase A complex. In subsite P_2, Arg 7 of RNase-4, like Lys 7 in RNase A molecule II, is within hydrogen bonding distance of atom O1A. The adenine ring of pdUppA-3′-p can occupy the B_2 subsite of RNase-4 by displacing three water molecules, and in the model forms the same stacking interactions with His 116 and hydrogen bond with Asn 66 as it does with the equivalent residues (His 119 and Asn 67) in the RNase A complex. However, atoms N6A and N7A of the adenine are ~0.6 Å beyond hydrogen bonding distance from the side chain atoms of Asn 70 (corresponding to Asn 71 in RNase A), and the interaction between N6A and Gln 69 of RNase A is not replicated due to the replacement of this residue by Lys 68 in RNase-4. At the same time, the adenosine ribose in the modeled complex engages in van der Waals interactions with Met 4 of RNase-4 that are not present in the complex with RNase A (which contains Ala at this position). The 5′-phosphate of pdUppA-3′-p is 4.4 Å away from atom Nζ of Lys 65 and could be involved in Coulombic interactions similar to those described for the RNase A−pdUppA-3′-p complex. These observations, together with the high affinity of pdUppA-3′-p for RNase-4 (*44*), suggest that the inhibitor might adopt a slightly different conformation upon binding to RNase-4 in order to optimize

its interactions with the enzyme in subsites B_1 and B_2. For example, changes in torsion angles α of uridine and ζ_{pp} and/or a different puckering of the uridine ribose [it is *C3′-exo* in d(Up) in contrast to *C2′-endo* in pdUppA-3′-p] might allow the uridine of pdUppA-3′-p to occupy the same position as that in the RNase-4−d(Up) complex and to engage in hydrogen bond interactions with Arg 101. Small conformational adjustments might also allow the adenosine to form additional hydrogen bonds within the B_2 subsite.

The model of the pdUppA-3′-p−RNase-4 complex suggests several ways in which more potent RNase-4 inhibitors might be constructed from the pdUppA-3′-p core. For example, insertion of a small spacer between the 5′-oxygen of the uridine and its phosphate group might enable the phosphate to form stronger interactions with the side chain of Lys 65 (hydrogen bonds rather than just medium-range Coulombic interactions). In addition, suitable groups attached to the 2′-position of the adenosine might be able to interact with Glu 108. In the RNase-4−pdUppA-3′-p model, the distance between atom O4U of uracil and one of the carboxylate oxygens of the C-terminus is 3.8 Å; hence, addition of a suitable group to O4U might generate new hydrogen bond interactions between the inhibitor and RNase-4. Also, a negatively charged group attached to O4U through a long spacer might be able to hydrogen bond with the side chain of Arg 102 which in the native crystal structure is involved in intermolecular interactions at the dimer interface. Such interactions, if they did not disrupt the hydrogen bonds of Arg 101, would enhance potency as well as specificity for RNase-4.

CONCLUSIONS AND IMPLICATIONS

The new compound examined here, pdUppA-3′-p, binds to the active site of RNase A and inhibits its ribonucleolytic activity more potently than any low molecular weight inhibitor previously known (*44*). The primary contacts of the inhibitor revealed by the crystal structure involve three of its substituents, i.e., the adenine ring, the 5′-*β*-phosphate, and the uracil ring. At one end, adenine hydrogen bonds to Asn 67, Gln 69, and Asn 71, and makes $\pi-\pi$ stacking interactions with the imidazole ring of His 119. At the other end, uracil forms hydrogen bonds with Thr 45, water-mediated interactions with Asp 83 and Ser 123, and stacking interactions with the phenyl ring of Phe 120. Between the two nucleosides, the 5′-*β*-phosphate makes hydrogen bonds with Gln 11, His 12, His 119, and Phe 120. In addition to these major anchoring contacts, the 5′- and 3′-terminal phosphates and the 5′-α-phosphate of the pyrophosphate linkage form less extensive interactions with the enzyme. Kinetic inhibition experiments have shown that the high affinity of pdUppA-3′-p for RNase A derives in large part from the unusual pyrophosphate linkage, which enhances binding by 300-fold compared to a monophosphate (*44*). This structural feature also confers higher affinity toward other members of the RNase superfamily such as EDN and RNase-4, which prefer pyrophosphate- vs monophosphate-linked dinucleotides by 130-fold and 790-fold, respectively (*44*).

From the present structural study, we can address two issues: (i) why the adenosine glycosyl bond torsion angle χ′ in these 5′-pyrophosphate nucleotides (pdUppA-3′-p, ppA-2′-p, ppA-3′-p) adopts a syn conformation; and (ii) why pdUppA-3′-p is a more potent inhibitor than ppA-3′-p. In the previous crystallographic studies of RNase complexes with $d(pA)_4$ (*69*), d(CpA) (*41*), d(ApTpApApG) (*40*), 2′,5′-d(CpA) (*42*), or d(UpcA) (*43*), the B_2 adenosine was found in an anti conformation. Indeed, it would be highly unfavorable for the adenosine in any of these complexes to adopt a syn conformation since this would not allow its 5′-phosphate to occupy the P_1 subsite or the pyrimidine base to reach the B_1 subsite. However, for the new class of inhibitors, it is the anti conformation and its associated placement of the 5′-α- rather than 5′-*β*-phosphate in P_1 that would be unfavorable, albeit for different reasons in the pdUppA-3′-p versus the ppA-3′-p and ppA-2′-p complexes. For pdUppA-3′-p, binding of the α-phosphate in P_1 would force the uridine out of B_1, thereby eliminating a substantial set of contacts. In the case of ppA-2′-p and ppA-3′-p, it seems likely that the *β*-phosphate can form stronger contacts than the α-phosphate with residues in the P_1 site because it carries a larger negative charge and its greater freedom of rotation would allow better optimization of hydrogen bond distances and angles (the α- and *β*-phosphates in pdUppA-3′-p have similar charge and flexibility). It is also possible that the interactions of RNase A with the syn adenosine might be even better than those normally formed with this nucleoside in its anti conformation. It is not clear which of these provides the driving force for the unusual binding mode of ppA-2′-p and ppA-3′-p: i.e., whether placement of the *β*- versus α-phosphate in P_1 is sufficiently advantageous so as to force the adenosine to adopt a (perhaps less favorable) syn conformation or whether the interactions of RNase A with a syn vs an anti adenosine are sufficiently advantageous so as to force the *β*-phosphate to occupy P_1.

pdUppA-3′-p is 9-fold more potent an inhibitor of RNase A than is ppA-3′-p, whereas dUppA-3′-p has been shown to be 2 times more effective than the earlier compound (*44*). The small improvement in binding of dUppA-3′-p compared to ppA-3′-p was proposed (*44*) to derive from a combination of positive factors associated with addition of the pyrimidine nucleoside—the enthalpic gain due to new interactions between uracil and the B_1 subsite and the entropic advantage of the increased structural constraints on the *β*-phosphate—which are partially counterbalanced by enthalpic losses due to this same conformational restriction of the *β*-phosphate, which would prevent this group from optimizing its interactions at P_1 as in the ppA-3′-p complex. The present pdUppA-3′-p−RNase A complex structure reveals four unexpected features that have bearing on this proposal: (i) the 5′-α-phosphate forms only a single hydrogen bond with RNase A in molecule I of the noncrystallographic dimer and none in molecule II, whereas it makes two and three hydrogen bonds in the respective molecules of the ppA-3′-p complex; (ii) an interaction between O5′A and Lys 7 in the ppA-3′-p complex has been lost; (iii) the 3′-phosphate of the adenosine hydrogen bonds with Lys 7 only in molecule I of the pdUppA-3′-p complex, whereas this interaction was seen in both molecules of the ppA-3′-p complex; and (iv) the hydrogen bonds at P_1 of the pdUppA-3′-p complex do not seem to be any less extensive or optimal than for the ppA-3′-p complex (in fact, Gln 11 makes a hydrogen bond with the *β*-phosphate of pdUppA-3′-p that was not observed in the earlier complex). Thus, in the pdUppA-3′-p complex (and most likely in the dUppA-3′-p complex as well), the negative

factors compensating for the added interactions at B_1 are more elaborate than had been suggested from modeling.

The 4.5-fold decrease in K_i upon addition of the 5′-phosphate to uridine in dUppA-3′-p (*44*) appears to be due to Coulombic interactions with Lys 66 in the P_0 subsite rather than to a hydrogen bond with this residue such as that in the modeled complex. The gain in binding energy, 0.9 kcal/mol, associated with the 5′-phosphate is reasonable for a Coulombic interaction over the ∼4.7 Å separating the two charged groups. Medium- and long-range Coulombic interactions have been shown to contribute significantly to binding of substrates to RNase A (*62*) and to influence catalysis by this enzyme as well (*70*). This type of interaction is also thought to stabilize the catalytic transition state of the serine protease subtilisin (*71*) and to enhance the rate of association of the superoxide anion to superoxide dismutase (*72*). Nevertheless, we cannot rule out the possibility that Lys 66 and the 5′-phosphate of pdUppA-3′-p form a hydrogen bond rather than just a charge−charge interaction in solution: relatively minor rotations of the phosphate and the Lys side chain would allow such a hydrogen bond to be made.

The RNase A−pdUppA-3′-p complex structure described here suggests ways for further rational design of tight binding inhibitors of this enzyme. Although the addition of uridine to the ppA-3′-p core has displaced five (molecule I) and three (molecule II) water molecules from the catalytic site, four other water molecules that mediate RNase−inhibitor interactions remain: three link uridine atoms O4U and O4′U with residues Val 43, Asp 83, and Ser 123, and another mediates between atom N1A and residues Asn 67 and Asp 121. These water molecules are also conserved in the structure of the RNase A−ppA-3′-p complex (*39*), and therefore indicate positions which are favorable for hydrogen bonds with RNase A. Thus, extensions of pdUppA-3′-p that place polar groups at these loci might replace weak water-mediated interactions with strong direct ones. Furthermore, the interactions of the terminal 5′- and 3′-phosphates, which appear to be suboptimal, might be enhanced by introducing suitable spacers to bring them closer to potential hydrogen-bonding partners.

Although the present complex structure is a step forward in our quest for potent RNase inhibitors, it also highlights that it is an unpredictable process. As discussed above, the increased inhibitory potency of pdUppA-3′-p was anticipated from the modeled complex (*44*), but the crystal structure of this complex reveals that the physical basis for the improvement differs from expectation in ways that have potentially important implications for the next stage of inhibitor design. These observations emphasize the importance of collecting structural data at each cycle in the iterative inhibitor design process where a significant enhancement in potency has been achieved.

ACKNOWLEDGMENT

We are grateful to the staff at the Synchrotron Radiation Source at Daresbury, England, and to Dr. Anastassios Papageorgiou and Ms. Evangelia Chrysina for help with X-ray data collection. We also thank Drs. M. N. G. James and S. Mosimann for EDN coordinates, Dr. G. L. Gilliland for the RNase−UpcA complex coordinates, Drs. S. S. Terzyan and M. Coll for the coordinates of free RNase-4 and RNase-4 in complex with d(Up), and Drs. Ester Boix and Daniel Holloway for helpful discussions and constructive criticisms of the manuscript. We thank Drs. James Riordan and Bert Vallee for advice and support.

REFERENCES

1. Durack, D. T., Ackerman, S. J., Loegering, D. A., and Gleich, G. J. (1981) *Proc. Natl. Acad. Sci. U.S.A. 78*, 5165−5169.
2. Fredens, K., Dahl, R., and Venge, P. (1982) *J. Allergy Clin. Immunol. 70*, 361−366.
3. Gleich, G. J., Loegering, D. A., Bell, M. P., Checkel, J. L., Ackerman, S. J., and McKean, D. J. (1986) *Proc. Natl. Acad. Sci. U.S.A. 83*, 3146−3150.
4. Fett, J. W., Strydom, D. J., Lobb, R. R., Alderman, E. M., Bethune, J. L., Riordan, J. F., and Vallee, B. L. (1985) *Biochemistry 24*, 5480−5486.
5. Olson, K. A., Fett, J. W., French, T. C., Key, M. E., and Vallee, B. L. (1995) *Proc. Natl. Acad. Sci. U.S.A. 92*, 442−446.
6. Soncin, F., Shapiro, R., and Fett, J. W. (1994) *J. Biol. Chem. 269*, 8999−9005.
7. Matoušek, J. (1973) *Experientia 29*, 858−859.
8. Soucek, J., Hruba, A., Paluska, E., Chudomel, V., Dostal, J., and Matoušek, J. (1983) *Folia Biol. 29*, 250−261.
9. Soucek, J., Chudomel, V., Potmesilova, I., and Novak, J. T. (1986) *Nat. Immun. Cell Growth Regul. 5*, 250−258.
10. Domachowske, J. B., Dyer, K. D., Adams, A. G., Leto, T. L., and Rosenberg, H. F. (1998) *Nucleic Acids Res. 26*, 3358−3363.
11. Domachowske, J. B., Dyer, K. D., Bonville, C. A., and Rosenberg, H. F. (1998) *J. Infect. Dis. 177*, 1458−1464.
12. Ackerman, S. J., Gleich, G. J., Loegering, D. A., Richardson, B. A., and Butterworth, A. E. (1985) *Am. J. Trop. Med. Hyg. 34*, 735−745.
13. Lehrer, R. I., Szklarek, D., Barton, A., Ganz, T., Hamann, K. J., and Gleich, G. J. (1989) *J. Immunol. 142*, 4428−4434.
14. Mikulski, S. M., Ardelt, W., Shogen, K., Bernstein, E. H., and Menduke, H. (1990) *J. Natl. Cancer Inst. 82*, 151−152.
15. Mikulski, S. M., Grossman, A. M., Carter, P. W., Shogen, K., and Costanzi, J. J. (1993) *Int. J. Oncol. 3*, 57−64.
16. Shapiro, R., Fett, J. W., Strydom, D. J., and Vallee, B. L. (1986) *Biochemistry 25*, 7255−7264.
17. Futami, J., Tsushima, Y., Murato, Y., Tada, H., Sasaki, J., Seno, M., and Yamada, H. (1997) *DNA Cell Biol. 16*, 413−419.
18. Egesten, A., Dyer, K. D., Batten, D., Domachowske, J. B., and Rosenberg, H. F. (1997) *Biochim. Biophys. Acta 1358*, 255−260.
19. Hofsteenge, J., Vicentini, A., and Zelenko, O. (1998) *Cell. Mol. Life Sci. 54*, 804−810.
20. Rosenberg, H. F., and Dyer, K. D. (1995) *Nucleic Acids Res. 23*, 4290−4295.
21. Shapiro, R., Fox, E. A., and Riordan, J. F. (1989) *Biochemistry 28*, 1726−1732.
22. Shapiro, R., and Vallee, B. L. (1989) *Biochemistry 28*, 7401−7408.
23. Curran, T. P., Shapiro, R., and Riordan, J. F. (1993) *Biochemistry 32*, 2307−2313.
24. Sorrentino, S., Glitz, D. G., Hamann, K. J., Loegering, D. A., Checkel, J. A., and Gleich, G. J. (1992) *J. Biol. Chem. 267*, 14859−14865.
25. Newton, D. L., Walbridge, S., Mikulski, S. M., Ardelt, W., Shogen, K., Ackerman, S. J., Rybak, S. M., and Youle, R. J. (1994) *J. Neurosci. 14*, 538−544.
26. Kim, J. S., Soucek, J., Matousek, J., and Raines, R. T. (1995) *Biochem. J. 308*, 547−550.
27. Wu, Y., Mikulski, S. M., Ardelt, W., Rybak, S. M., and Youle, R. (1993) *J. Biol. Chem. 268*, 10686−10693.
28. Boix, E., Wu, Y. N., Vasandani, V. M., Saxena, S. K., Ardelt, W., Ladner, J., and Youle, R. J. (1996) *J. Mol. Biol. 257*, 992−1007.
29. Vescia, S., Tramontano, D., Augusti-Tocco, G., and D'Alessio, G. (1980) *Cancer Res. 40*, 3740−3744.

30. Richards, F. M., and Wyckoff, H. W. (1971) *Enzymes (3rd Ed.) 4*, 647−806.
31. Eftink, M. E., and Biltonen, R. L. (1987) in *Hydrolytic Enzymes*, pp 333−376, Elsevier Science Publishers, Amsterdam, New York, and Oxford.
32. Richardson, R. M., Parés, X., and Cuchillo, C. M. (1990) *Biochem. J. 267*, 593−599.
33. Parés, X., Nogués, M. V., Llorens, R., and Cuchillo, C. M. (1991) *Essays Biochem. 26*, 89−103.
34. Boix, E., Nogués, M. V., Schein, C. H., Benner, S. A., and Cuchillo, C. M. (1994) *J. Biol. Chem. 269*, 2529−2534.
35. Cuchillo, C. M., Vilanova, M., and Nogués, M. (1997) in *Ribonucleases: Structure and function* (D'Alessio, G., and Riordan, J. F., Eds.) pp 271−304, Academic Press, Inc., New York.
36. Nogués, M. V., Moussaoui, M., Boix, E., Vilanova, M., Ribo, M., and Cuchillo, C. M. (1998) *Cell. Mol. Life Sci. 54*, 766−774.
37. Raines, R. T. (1998) *Chem. Rev. 98*, 1045−1065.
38. Russo, N., Shapiro, R., and Vallee, B. L. (1997) *Biochem. Biophys. Res. Commun. 231*, 671−674.
39. Leonidas, D. D., Shapiro, R., Irons, L. I., Russo, N., and Acharya, K. R. (1997) *Biochemistry 36*, 5578−5588.
40. Fontecilla-Camps, J. C., de Llorens, R., le Du, M. H., and Cuchillo, C. M. (1994) *J. Biol. Chem. 269*, 21526−21531.
41. Zegers, I., Maes, D., Dao-Thi, M.-H., Poortmans, F., Palmer, R., and Wyns, L. (1994) *Protein Sci. 31*, 2322−2339.
42. Toiron, C., Gonzalez, C., Bruix, M., and Rico, M. (1996) *Protein Sci. 5*, 1633−1647.
43. Gilliland, G. (1997) in *Ribonucleases: Structure and functions* (D'Allesio, G., and Riordan, J. F., Eds.) pp 305−341, Academic Press, Inc., New York.
44. Russo, N., and Shapiro, R. (1999) *J. Biol. Chem. 274*, 14902−14908.
45. Otwinowski, Z., and Minor, W. (1997) in *Methods in Enzymology* (Carter, C. W. J., and Sweet, R. M., Eds.) pp 307−326, Academic Press, New York.
46. Brünger, A. T., Krukowski, J., and Erickson, J. (1990) *Acta Crystallogr. A46*, 585−593.
47. Ladner, J. E., Wladkoswki, B. D., Svensson, L. A., Sjolin, L., and Gilliland, G. L. (1997) *Acta Crystallogr. D53*, 290−301.
48. Brünger, A. T. (1992) *Nature 355*, 472−475.
49. Moodie, S. L., and Thornton, J. M. (1993) *Nucleic Acids Res. 21*, 1369−1380.
50. Ke, H. M., Zhang, Y. P., and Lipscomb, W. N. (1990) *Proc. Natl. Acad. Sci. U.S.A. 87*, 5243−5247.
51. Wladkowski, B. D., Svensson, L. A., Sjolin, L., Ladner, J. E., and Gilliland, G. L. (1998) *J. Am. Chem. Soc. 120*, 5488−5498.
52. Gilliland, G. L., Dill, J., Pechik, I., Svensson, L. A., and Sjolin, L. (1994) *Protein Pept. Lett. 1*, 60−65.
53. Wlodawer, A., Miller, M., and Sjolin, L. (1983) *Proc. Natl. Acad. Sci. U.S.A. 80*, 3628−3631.
54. delCardayre, S. B., and Raines, R. T. (1994) *Biochemistry 33*, 6031−6037.
55. delCardayre, S. B., and Raines, R. T. (1995) *J. Mol. Biol. 252*, 328−336.
56. Sawada, F., and Irie, M. (1969) *J. Biochem. (Tokyo) 66*, 415−418.
57. Li, J. R., and Walz, F. G. (1974) *Arch. Biochem. Biophys. 161*, 227−233.
58. Iwahashi, K., Nakamura, K., Mitsui, Y., Ohgi, K., and Irie, M. (1981) *J. Biochem. (Tokyo) 90*, 1685−1690.
59. deLlorens, R., Arus, C., Pares, X., and Cuchillo, C. M. (1989) *Protein Eng. 2*, 417−429.
60. Beintema, J. J., Schuller, C., Irie, M., and Carsana, A. (1988) *Prog. Biophys. 51*, 165−192.
61. Beintema, J. J. (1989) *FEBS Lett. 254*, 1−4.
62. Fisher, B. M., Ha, J. H., and Raines, R. T. (1998) *Biochemistry 37*, 12121−12132.
63. Mosimann, S. C., Newton, D. L., Youle, R. J., and James, M. N. G. (1996) *J. Mol. Biol. 260*, 540−552.
64. Terzyan, S. S., Peracaula, R., deLlorens, R., Tsushima, Y., Yamada, H., Seno, M., Gomis-Ruth, F. X., and Coll, M. (1999) *J. Mol. Biol. 285*, 205−214.
65. Borkakoti, N., Moss, D. A., and Palmer, R. A. (1982) *Acta Crystallogr. B38*, 2210−2217.
66. deMel, V. S. J., Doscher, M. S., Martin, P. D., and Edwards, B. F. P. (1994) *FEBS Lett. 349*, 155−160.
67. Löffler, A., Doucey, M. A., Jansson, A. M., Möller, D. R., de Beer, T., Hess, D., Meldal, M., Richter, W. J., Vliegenthart, J. F. G., and Hofsteenge, J. (1996) *Biochemistry 35*, 12005−12014.
68. Hofsteenge, J., Moldow, C., Vicentini, A. M., Zelenko, O., Jarai-Kote, Z., and Neumann, U. (1998) *Biochemistry 37*, 9250−9257.
69. McPherson, A., Brayer, G. D., and Morrison, R. D. (1986) *J. Mol. Biol. 189*, 305−327.
70. Fisher, B. M., Schultz, L. W., and Raines, R. T. (1998) *Biochemistry 37*, 17386−17401.
71. Jackson, S. E., and Fersht, A. R. (1993) *Biochemistry 32*, 13909−13916.
72. Sharp, K., Fine, R., and Honig, B. (1987) *Science 236*, 1460−1463.
73. IUPAC−IUB (1983) *Eur. J. Biochem. 131*, 9−15.
74. Altona, C., and Sundaralingam, M. (1972) *J. Am. Chem. Soc. 94*, 8205−8212.
75. McDonald, I. K., and Thornton, J. M. (1994) *J. Mol. Biol. 238*, 777−793.
76. Read, J. (1986) *Acta Crystallogr. A 42*, 140−149.
77. Nicholls, A., and Honig, B. (1991) *J. Comput. Chem. 12*, 435−445.
78. Kraulis, P. J. (1991) *J. Appl. Crystallogr. 24*, 946−950.

BI990900W